Available online at www.sciencedirect.com
ScienceDirect
Nuclear Medicine and Biology 38 (2011) 807–817
NUCLEAR MEDICINE — AND — BIOLOGY
www.elsevier.com/locate/nucmedbio

New radiosynthesis of 2-deoxy-2-[^{18}F]fluoroacetamido-D-glucopyranose and its evaluation as a bacterial infections imaging agent

Miguel E. Martínez[a], Yasushi Kiyono[a,*], Sakon Noriki[b], Kunihiro Inai[c], Katheryn S. Mandap[a], Masato Kobayashi[a,e], Tetsuya Mori[a], Yuji Tokunaga[d], Vijay N. Tiwari[a], Hidehiko Okazawa[a], Yasuhisa Fujibayashi[a,f], Tatsuo Ido[a,g]

[a]*Biomedical Imaging Research Center, University of Fukui, Eiheiji, Yoshida, Fukui, 910-1193, Japan*
[b]*Department of Tumor Pathology, University of Fukui, Fukui, 910-1193, Japan*
[c]*Department of Molecular Pathology, University of Fukui, Fukui, 910-1193, Japan*
[d]*Department of Materials Science and Engineering, University of Fukui, Fukui, 910-8507, Japan*
[e]*School of Health Sciences, College of Medical, Pharmaceutical and Health Sciences, Kanazawa University, Kanazawa, 920-0942, Japan*
[f]*Molecular Imaging Center, National Institute of Radiological Sciences, Chiba, 263-8555, Japan*
[g]*Japan Radioisotope Association, Tokyo, 113-8941, Japan*

Received 5 November 2010; received in revised form 25 January 2011; accepted 12 February 2011

Abstract

Introduction: The diagnosis of infection and the ability to distinguish bacterial infection from nonbacterial inflammation by positron emission tomography (PET) have gained interest in recent years, but still few specific radiopharmaceuticals are available for use. In this study, we developed a new radiosynthesis method of 2-deoxy-2-[^{18}F]fluoroacetamido-D-glucopyranose ([^{18}F]FAG) by applying microwave irradiation and demonstrated that [^{18}F]FAG could be a potential radiopharmaceutical to distinguish bacterial infection from nonbacterial inflammation.

Methods: 1,3,4,6-Tetra-*O*-acetyl-2-deoxy-2-bromoacetamido-D-glucopyranose was used as precursor, and labeling was performed under microwave irradiation conditions followed by alkaline hydrolysis and high-performance liquid chromatography (HPLC) purification. In vitro uptake of [^{18}F]FAG by *Escherichia coli* was performed. Tissue biodistribution of [^{18}F]FAG was performed in mice. Moreover, PET imaging acquisition of *E. coli* infection and nonbacterial inflammation models was performed in rats. Tissue radiotracer-accumulated sites were analyzed by hematoxylin and eosin staining and anti–*E.coli* immunostaining.

Results: The radiosynthesis of [^{18}F]FAG was achieved with microwave irradiation, and the radiochemical yield was 9.7%±2.8% end of bombardment (EOB); the radiochemical purity was more than 98%, and the total synthesis time was 62 min. Compared with control group, in vitro uptake of [^{18}F]FAG by *E. coli* was significantly decrease in inhibition group ($P<.05$). Biodistribution studies in mice showed rapid clearance of [^{18}F]FAG from the animal body. [^{18}F]FAG clearly visualized the infection areas but not nonbacterial inflammation areas in PET studies. Quantitative analysis revealed that the uptake of [^{18}F]FAG into infection areas was significantly higher than that of [^{18}F]FAG into inflammation areas ($P<.05$). Histological analysis demonstrated the presence of bacterial cells at the sites of accumulation of [^{18}F]FAG.

Conclusions: Using 1,3,4,6-tetra-*O*-acetyl-2-deoxy-2-bromoacetamido-D-glucopyranose as a precursor, the new radiosynthesis method of [^{18}F]FAG was achieved in fewer steps and with a shorter synthesis time than previously reported. Furthermore, [^{18}F]FAG was able to distinguish bacterial infection from nonbacterial inflammation.

Keywords: Infection; Inflammation; Bacterial imaging agent; PET; Glucosamine derivatives

1. Introduction

Although there have been significant advances in our understanding of the pathogenesis of infection, infection still remains a major cause of patient morbidity and mortality

* Corresponding author. Tel.: +81 776 61 8420; fax: +81 776 61 8170.
E-mail address: ykiyono@u-fukui.ac.jp (Y. Kiyono).

0969-8051/$ – see front matter © 2011 Elsevier Inc. All rights reserved.
doi:10.1016/j.nucmedbio.2011.02.006

throughout the world [1]. It is essential for the efficient treatment of infection and prevention of complications to distinguish bacterial infection from nonbacterial inflammation [2]. Most infections are diagnosed by clinical history, physical examination, microbiological analyses of samples derived from the infected tissue and imaging techniques. Although modern imaging techniques such as computed tomography and magnetic resonance imaging can provide excellent structural resolution in chronic stages of infection, these modalities have limitations in distinguishing bacterial infection from nonbacterial inflammation [3]. Positron emission tomography (PET) or single-photon emission computed tomography can detect earlier the physiological and biochemical changes at the site of lesions. Therefore, nuclear medicine with its powerful imaging techniques can help to distinguish bacterial infection from nonbacterial inflammation. The development of new radiopharmaceuticals for PET may be helpful in identifying infected structures, and the potential of PET for quantification could have further implications for prediction and monitoring of therapeutic response [4].

Amino sugars are versatile components of the cell surface structures of bacteria. They form the essential backbone of the peptidoglycan in both gram-positive and gram-negative bacteria and are also constituents of the outer membrane lipopolysaccharide layer and the polysaccharide capsules of gram-negative bacteria. The peptidoglycan is the main component of the bacteria cell wall and is built from alternating units of *N*-acetylglucosamine and *N*-acetylmuramic acid, cross-linked with oligopeptides at the lactic acid residue of *N*-acetylmuramic acid. The pathway for the metabolism of *N*-acetylglucosamine and the biosynthetic pathway producing uridine diphosphate-*N*-acetylglucosamine for incorporation into cell wall components have been described elsewhere [5,6]. The incorporation of a positron emitter into *N*-acetylglucosamine structure could make this compound a specific bacterial imaging agent for PET. Although a variety of *N*-acetylglucosamine derivatives have been synthesized and studied for their roles as plasma-membrane modifiers, tumor chemotherapeutic or imaging agents [7–9], there are no studies of bacterial infections imaging by the use of positron-labeled *N*-acetylglucosamine derivatives [10].

In this study, we developed a new radiosynthesis method of [^{18}F]FAG by applying microwave irradiation and demonstrated that [^{18}F]FAG could be a potential radiopharmaceutical to distinguish bacterial infection from nonbacterial inflammation.

2. Materials and methods

2.1. Reagents

All reagents, unless otherwise specified, were obtained from Nacalai Tesque (Kyoto, Japan), and were used without further purification. Anhydrous acetonitrile, anhydrous pyridine, anhydrous dichloromethane, 1,10-diaza-4,7,13,16,21,24-hexaoxabicyclo[8.8.8]hexacosane (K_{222}), potassium carbonate and D-glucosamine hydrochloride were obtained from Sigma-Aldrich (St. Louis, MO, USA). high-performance liquid chromatography-grade anhydrous acetonitrile was obtained from Kanto Chemical (Tokyo, Japan). Cyclophosphamide monohydrate (CPA) and anhydrous magnesium sulfate were purchased from WAKO Pure Industries (Osaka, Japan).

2.2. Bacterial strain and culture

From the point of view of safety, availability and easy handling, *Escherichia coli* (*E. coli*) was chosen as a model of bacteria. *E. coli* (ATCC No. 8739) was purchased from Kanto Chemical. A single colony of bacteria collected from an Luria-Bertani (LB)' agar plate was first grown overnight in 5 ml of LB' broth at 37°C and 200 rpm. Afterward, 50 μl of the aliquot was resuspended in 2 ml of fresh heart infusion broth and incubated for additional 4 h until a logarithmic multiplication was observed. Bacteria were centrifuged and washed with warmed phosphate-buffered saline before being adjusted to a final concentration of 1×10^7 colony-forming unit.

2.3. General methods

Melting points (uncorrected) were determined on a ATM-01 flat type apparatus (As One, Tokyo, Japan). Thin-layer chromatography (TLC) was performed on glass back plates coated with silica gel 60 F_{254} (Merck, Darmstadt, Germany). The following solvent systems were used: (A) 9:1 $CHCl_3/CH_3OH$ or (B) 5:4:2:1 *n*-butanol/CH_3OH/ammonia 28%/H_2O. Samples were visualized by spraying the plates with 5% H_2SO_4 in ethanol and heating or reading radioactivity in a AR-2000 Imaging scanner (Bioscan, Washington DC, USA). Flash chromatography was performed on a Yamazen YFLC (Yamazen, Tokyo, Japan) system. Infrared (IR) spectra were recorded on a Horiba FT-720 spectrometer (Horiba, Tokyo, Japan) and nuclear magnetic resonance (NMR) measurements were determined on a JEOL LA-500 spectrometer (JEOL, Tokyo, Japan) (500 MHz for ^{1}H and 125 MHz for ^{13}C). Samples were dissolved in $CDCl_3$, and Me_4Si was used as the internal reference. Elemental analyses were performed on a CHN CORDER MT-6 Elemental analyzer (Yanaco, Tokyo, Japan). Reverse-phase HPLC was performed using a Shimadzu (Shimadzu, Kyoto, Japan) system equiped with a refractive index detector and Ludlum 44-10 NaI (Tl) radioactive detector (Ludlum Measurements; Sweetwater, TX, USA). A Capintec Radiosotope Calibrator (CRC-12 Capintec Instruments Inc., Ramsey, NJ, USA) was used for all radioactivity measurements unless otherwise stated.

2.4. Synthesis of 1,3,4,6-tetra-O-acetyl-2-deoxy-2-bromoacetamido-D-glucopyranose

2.4.1. 1,3,4,6-Tetra-O-acetyl-2-deoxy-2-amino-D-glucopyranose hydrochloride (**4**)

1,3,4,6-Tetra-*O*-acetyl-2-deoxy-2-amino-*D*-glucopyranose hydrochloride was prepared following the method

described by Myszka et al. [11]. mp 220°C (decomposed), IR (KBr)ν: 3432 (NH_2), 1751 (C=O, Ac) cm^{-1}, ^{1}H-NMR (D_2O, 500 MHz) δ: 5.95 (d, 1 H, *J* 8.6 Hz), 5.47 (dd, 1H, *J* 10.7 and 9.2 Hz), 5.17–5.09 (m, 1H), 4.38–4.33 (m, 1H), 4.24–4.18 (m, 2H), 3.77 (dd, 1H, *J* 10.6 and 8.6 Hz), 2.21, 2.13, 2.089 and 2.086 (s, 3H×4).

2.4.2. 1,3,4,6-Tetra-O-acetyl-2-deoxy-2-amino-D-glucopyranose (5)

To a solution of **4** (7.2 g, 19 mmol) in water (85 ml) was slowly added sodium acetate (1.86 g, 23 mmol) under vigorous stirring. After crystallization began, the mixture was stirred for approximately 1.5 h at room temperature. The precipitate was extracted with dichloromethane, the organic phase was dried over $MgSO_4$ and the solvent was evaporated. Addition of acetone to the residue followed by Et_2O caused precipitation of **5** as a white solid to give 5.7 g (81%), which was further recrystallized from ethanol. mp 149–150°C; IR ($CHCl_3$)ν: 3363 (NH), 1741 (C=O, Ac) cm^{-1}, ^{1}H-NMR ($CDCl_3$, 500 MHz) δ: 5.51 (d, 1 H, *J* 8.6 Hz), 5.07–5.02 (m, 2H), 4.31 (dd, 1H, *J* 12.2 and 4.4 Hz), 4.08 (dd, 1H, *J* 12.5 and 2.1 Hz), 3.85–3.80 (m, 1H), 3.10–3.04 (m, 1H), 2.18, 2.09, 2.08 and 2.03 (s, 3H×4).

2.4.3. 1,3,4,6-Tetra-O-acetyl-2-deoxy-2-(bromoacetamido)-D-glucopyranose (6)

To a cooled solution of **5** (0.7 g, 2.0 mmol) in a mixture of dry dichloromethane (10 ml) and dry pyridine (1 ml) was added dicyclohexylcarbodiimide (0.45 g, 2.2 mmol) followed by bromoacetic acid (0.3 g, 2.2 mmol). The mixture was stirred in an ice/water bath for 2 h. After filtration, the filtrate was discarded and the solution washed with water, diluted hydrochloric acid and again with water. The organic layer was dried over $MgSO_4$ and filtered, the solvent was evaporated to dryness and the residue was recrystallized from ethanol. mp 169–170°C; IR ($CHCl_3$)ν: 3357 (NH), 1754 (C=O, Ac) cm^{-1}, ^{1}H-NMR ($CDCl_3$, 500 MHz) δ: 6.56 (d, 1H, *J* 9.5 Hz), 5.79 (d, 1H, *J* 8.5 Hz), 5.30 (dd, 1H, *J* 10.7 and 9.2 Hz), 5.13 (t, 1H, *J* 9.6 Hz), 4.31–4.22 (m, 2H), 4.14 (dd, 1H, *J* 12.5 and 2.1 Hz), 3.90–3.85 (m, 1H), 3.78 (s, 2H), 2.12, 2.10, 2.061 and 2.057 (s, 3H×4). ^{13}C-NMR ($CDCl_3$, 125 MHz) δ: 170.96, 170.63, 169.33, 169.31, 166.33, 92.1, 72.89, 71.90, 67.85, 61.62, 53.52, 28.20, 20.87, 20.69, 20.64, 20.56. Anal. Calcd for $C_{16}H_{22}BrNO_{10}$: C, 41.04; H, 4.74; N, 2.99. Found: C, 40.97; H, 4.68; N, 3.02.

With the purpose of use for analysis and quality controls during radiosynthesis, 1,3,4,6-tetra-*O*-acetyl-2-deoxy-2-fluoroacetamido-D-glucopyranose was synthesized by a similar procedure as for compound **6** using fluoroacetic acid generated in situ; mp 196–198°C; IR (KBr)ν: 1754 (C=O, Ac) cm^{-1}, ^{1}H−NMR ($CDCl_3$, 500 MHz) δ: 6.57 (d, 1H, *J* 9.5 Hz), 5.79 (d, 1H, *J* 8.5 Hz), 5.27 (dd, 1H, *J* 10.7 and 9.3 Hz), 5.15–5.08 (m, 1H), 4.78 (dd, 1H, *J* 17.7 and 14.7 Hz), 4.68 (dd, 1H, *J* 17.7 and 14.7 Hz), 4.32–4.22 (m, 2H), 4.11 (dd, 1H, *J* 12.5 and 2.1 Hz), 3.86–382 (m, 1H), 2.10; 2.07, 2.024 and 2.020 (s, 3H × 4). ^{13}C-NMR ($CDCl_3$, 125 MHz) δ: 170.88, 170.64, 169.31, 168.01, 167.87, 92.1, 79.93 (d, J_{C-F} 186 Hz), 72.82, 72.12, 67.80, 61.58, 52.59, 20.84, 20.70, 20.56 and 20.54.

2.5. Radiosynthesis of [^{18}F]FAG

All reactions were performed in a semiautomated system [12] with a CEM Discover (Matthews, NC, USA) single-mode microwave reactor system. This system is capable to deliver continuously microwave power with selectable power output (0–300 W) and a programmable temperature from 25°C to 250°C. It is equipped with an infrared temperature control system located below the microwave cavity floor that monitors and controls the temperature conditions of the reaction vessel. The temperature sensor is used in a feedback loop with the magnetron to regulate the power output that maintains the temperature set point. No carrier added [^{18}F]fluoride was produced in a RDS eclipse RD/HP cyclotron (Siemens/CTI, Knoxville, TN, USA) via the ^{18}O(p,n)^{18}F reaction using ^{18}O-enriched water. After irradiation, the enriched water was trapped into a SepPak Light QMA cartridge (Waters, Milford, MA, USA) pretreated with 1 ml of 0.2 M K_2CO_3 and 10 ml of water. The [^{18}F]fluorine trapped on the column was eluted with a solution of K_2CO_3/K_{222} in acetonitrile/water (96:4) based on a previous report [13]. The resulting $[K/K_{222}]^{+18}F^-$ solution was then evaporated at 110°C in a stream of argon gas (20 ml/min) using an average microwave power of about 150 W. To the dried $[K/K_{222}]^{+18}F^-$ complex, a solution of bromide precursor (**6**) in anhydrous CH_3CN was added, and experiments were conducted (under closed system reaction) to optimize different variables including labeling temperature, reaction time and precursor amount. During optimization of the radiofluorination, samples from the crude product were measured for incorporation yield using radio TLC, and the result obtained was corrected based on the percent distribution of the radioactivity obtained in the reaction mixture. The mixture was then evaporated at 70°C under argon flow until 0.1–0.2 ml remained. The hydrolysis conditions at room temperature using 1 ml of sodium hydroxide was optimized considering base concentration and reaction time. The final solution was neutralized by the addition of 2 M hydrochloric acid before purification in the HPLC system. The radioactive mixture was purified by HPLC (Cosmosil sugar-D column, 10 mm internal diameter (ID)×250 mm, CH_3CN/H_2O 80:20, 3 ml/min, 210 nm), and the radioactivity peak corresponding to [^{18}F]FAG was then directly transferred to a solvent replacement unit (JFE Holdings, Tokyo, Japan) wherein removal of the solvent system was performed in vacuum. The residue was then redissolved in 1 ml of normal saline solution. The final radiochemical purity and stability of [^{18}F]FAG were determined by radio TLC (solvent B) and HPLC (Cosmosil sugar-D column 4.6 mm ID×150 mm, CH_3CN/H_2O 80:20, 1 ml/min, 210 nm). The R_f value of [^{18}F]FAG was determined at 0.30, and the retention time for the peak was detected at

3.2 min; both were confirmed with a FAG cold standard synthesized in our laboratory.

2.6. In vitro E. coli uptake study

E. coli grown in medium heart infusion broth was divided in control and inhibition groups, and aliquots of 1 ml by triplicate were used for time points. In inhibition group, glucosamine at a final concentration of 10 mg/ml was added. After the addition of 0.37 MBq of [^{18}F]FAG in saline, solution samples were incubated at 37°C. After 30- and 120-min incubation, samples were washed three times with ice-cold phosphate-buffered saline (−), and then 500 μl of lysis buffer was added. Aliquots of each sample were counted in a 1480 Automatic Gamma Counter (Perkin Elmer, Osaka, Japan). The contents of protein was measured by bicinchoninic acid Protein Assay Kit following the instruction manual (Pierce Biotechnology, Rockford, IL, USA).

2.7. Animal studies

All animal experiments were approved by the animal care committee at the University of Fukui and conducted in accordance with the international standards for animal welfare and institutional guidelines. Adequated measures were taken to minimize pain or discomfort. Animals were housed under a 12-h light/12-h dark cycle with free access to food and water.

2.8. Biodistribution study

For the biodistribution study, 0.37 MBq of [^{18}F]FAG was injected into male ddY mice (n=30, 28–30 g, 6 weeks; Japan SLC, Shizuoka, Japan) via the tail vein. Following the injection, animals were killed under light ether anesthesia, and heparinized blood was obtained at 5, 10, 15, 30, 60 and 90 min (n=5 each point). The organs and tissues were removed, weighed and counted in a 1480 Automatic Gamma Counter (Perkin Elmer). Tissue radioactivity was expressed as percentage injected dose per gram of tissue:

$$\%\text{dose/g} = \frac{[\text{counts of tissue counts}]/[\text{injection counts}]}{[\text{gram of tissue}]} \times 100$$

2.9. Induction of E. coli infections in rats

Healthy male Sprague-Dawley rats (n=5, 80–90 g, 5 weeks; Japan SLC) were used for the induction of experimental infections. A week before PET acquisition image, the animals were immunosuppressed with an intraperitoneal injection of 180 mg/kg of CPA. Four days later, approximately 1×10^7 colony-forming units of bacteria were administered into the right front leg muscle followed by additional immunosuppression using 90 mg/kg of CPA on the next day. All animals developed a detectable abscess, and 2 days later, animals were used for PET experiments.

2.10. Induction of inflammatory process in rats

Healthy male Sprague-Dawley rats (n=5, 140–160 g, 6 weeks; Japan SLC) were used for the induction of experimental inflammation. Aseptic inflammation was induced 24 h before PET image acquisition with 100 μl of 100% pure turpentine oil inoculated into the right front leg muscle under ether anesthesia.

Before PET image acquisition, animals were fasted with no food overnight but with water supplied ad libitum. All animals developed an abscess detectable as a palpable fluctuant mass by either method bacterial infection or aseptic inflammation. The abscess sizes in both groups measured using a slide gauge were similar and within a range of 1.5–2.0 cm.

2.11. Small animal PET imaging

PET imaging of infection or inflammation in rat was performed using a small animal PET scanner (SHR-41000; Hamamatsu Photonics, Hamamatsu, Japan) [14]. The scanner acquires 213 slices covering an axial length of 160 mm, with a three-dimension mode and achieving a resolution of 2.0–2.5 mm full width at half maximum in the transaxial direction and 2.8 mm full width at half maximum in the axial direction. One hour before scanning, animals were injected with 16.7–22.2 MBq of radiotracer ([^{18}F]FAG or [^{18}F]FDG) via the tail vein. The animals were placed in the prone position in the PET scanner and then maintained under 2%–3% isoflurane (Abbott, Tokyo, Japan) air inhalation during image acquisition. Static PET images were acquired without attenuation correction over a 30-min period. Then regions of interest in three consecutive frames were drawn manually over the right front leg muscle and the contralateral nontarget left front leg muscle for each animal. [^{18}F]FAG and [^{18}F]FDG uptake over infected or inflamed areas was quantified using Dr. View Software, version 2.0.0 (JAS, Tokyo, Japan). Finally, utilizing the mean value, all regions of interests were converted to standardized uptake values (SUV).

$$\text{SUV} = \frac{[\text{tissue acitivity concentration}]}{([\text{injection dose}]\,/\,[\text{body weight}])}$$

After PET imaging, the animals were killed, and the resected tissues were fixed with 20% formalin for pathological examinations.

2.12. Histology

The slide sections thin-sliced from the paraffin-embedded block were stained with hematoxylin and eosin dye or with primary anti–*E. coli* polyclonal antibody (DAKO, Japan) as described [15]. A Histofine SAB-PO kit (Nichirei, Tokyo, Japan) was used for the secondary reaction of immunostaining. The obtained sections were pathologically evaluated by two different pathologists specializing in the pathophysiological analysis of infectious diseases.

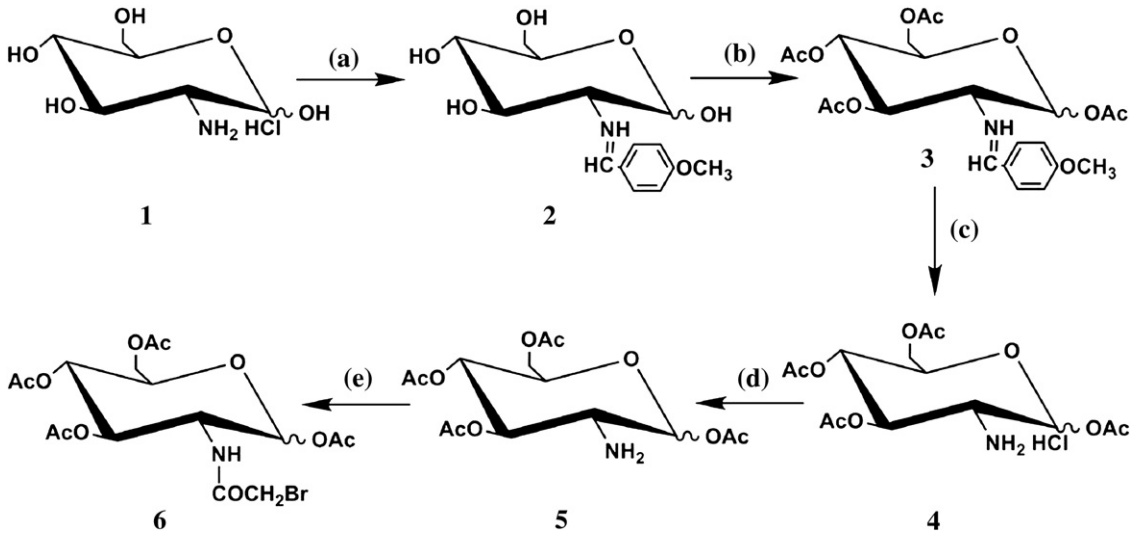

Fig. 1. Synthesis scheme of TA-BrAG. Chemical names: D-glucosamine hydrochloride (**1**), 2-deoxy-2-[*p*-methoxybenzylidene(amino)]-D-glucopyranose (**2**), 1,3,4,6-tetra-*O*-acetyl-2-deoxy-2-[*p*-methoxybenzylidene(amino)]-D-glucopyranose (**3**), 1,3,4,6-tetra-*O*-acetyl-2-deoxy-2-amino-D-glucopyranose hydrochloride (**4**), 1,3,4,6-tetra-*O*-acetyl-2-deoxy-2-amino-D-glucopyranose (**5**), 1,3,4,6-tetra-*O*-acetyl-2-deoxy-2-(bromoacetamido)-D-glucopyranose (**6**). Reagents and conditions: aq NaOH, *p*-anisaldehyde (a); Py, Ac_2O (b); acetone, 5 M HCl (c); water, AcONa (d); DCC, $BrCH_2COOH$, CH_2Cl_2/Py (e).

2.13. Statistical analysis

Unpaired *t* test was applied for two group comparison in *E. coli* uptake study. SUV differences between groups were tested for statistical significance using one-way analysis of variance with a post hoc Newman–Keuls multiple-comparison test. A probability value of less than .05 was considered to indicate a significant difference. Results are expressed as mean±S.D.

3. Results

3.1. Radiosynthesis of [^{18}F]FAG

The steps of the new synthesis scheme for 1,3,4,6-tetra-*O*-acetyl-2-deoxy-2-bromoacetamido-D-glucopyranose (TA-BrAG) are summarized in Fig. 1. The final TA-BrAG obtained by this route was used as a precursor for the synthesis of [^{18}F]FAG by nucleophilic substitution with [^{18}F]fluoride anion (Fig. 2).

We investigated several microwave reaction conditions in order to optimize the [^{18}F]F^- incorporation rate into TA-BrAG precursor, including the effects of reaction temperature, microwave irradiation time and amount of TA-BrAG precursor (Table 1). First, using 29.4 mg (62.5 μmol) of TA-BrAG dissolved in 0.5 ml of anhydrous acetonitrile, we studied the incorporation yields at 90°C, 100°C and 110°C (series 1∼3). The optimum labeling temperature was determined to be at 100°C with an average microwave power of around 30 W. The lower yield observed at higher temperatures may be attributed to degradation of TA-[^{18}F]FAG. Next, the optimal amount of precursor was evaluated (series 4∼8). Five different molar ratios of TA-BrAG precursor/K_{222} were examined (0.5, 1, 2, 3 and 5). The incorporation yield by varying the amount of TA-BrAG precursor keeping the K_{222} constant showed no significant increase in incorporation yield while varying the ratio of TA-BrAG precursor/K_{222} from 2 up to 5. In consequence, the minimal amount of TA-BrAG precursor, which corresponds to an amount of 11.7 mg (TA-BrAG precursor/K_{222} ratio of 2) was selected. Finally, we investigated the incorporation yields using five different reaction times (1.5, 3, 5, 10 and 20 min) (series 9∼13). A reaction time of 10 min was enough to obtain the highest incorporation yields. In summary, utilizing 11.7 mg of TA-BrAG in acetonitrile reacted at 100°C and using an average microwave power of 30 W gave an incorporation yield of 75.5%±4.2% (*n*=3) in 10-min time.

For optimization of the hydrolysis of the *O*-acetyl groups of the TA-[^{18}F]FAG, the reaction time and concentrations of

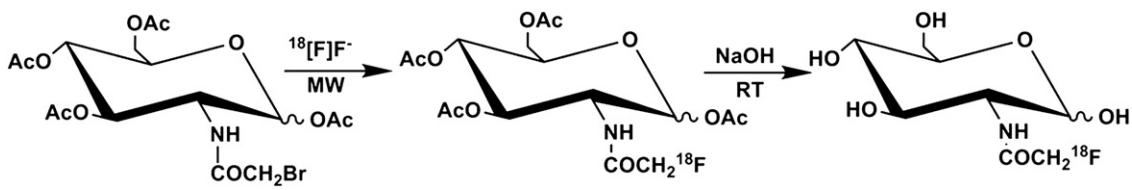

Fig. 2. Radiosynthesis scheme of [^{18}F]FAG.

Table 1
Summary of microwave fluorination optimization

Series	TA-BrAG (mg)	Reaction temperature (°C)	Molar ratio TA-BrAG/K_{222} sln	Reaction time (min)	%TA-[^{18}F]FAG yield (RTLC)[a]
1	29.4	90	5	10	63.7±0.7
2	29.4	100	5	10	75.4±1.8
3	29.4	110	5	10	57.9±11.4
4	2.9	100	0.5	10	48.3±7.8
5	5.8	100	1	10	62.8±5.4
6	11.7	100	2	10	75.5±4.2
7	17.5	100	3	10	76.6±7.5
8	29.4	100	5	10	77.3±2.5
9	11.7	100	2	1.5	58.6±2.9
10	11.7	100	2	3	61.3±1.6
11	11.7	100	2	5	64.4±5.1
12	11.7	100	2	10	75.5±4.2
13	11.7	100	2	20	70.4±2.2

[a] Values represent the mean±S.D. (n=3).

sodium hydroxide were examined (Table 2). The hydrolysis of TA-[^{18}F]FAG was feasible in liquid phase at room temperature. The maximum yield of [^{18}F]FAG was obtained with 1 M sodium hydroxide for 1 min. The TA-[^{18}F]FAG was reproducibly converted into [^{18}F]FAG under these conditions with an average recovery of 30%–40%.

After the optimization described above, we developed the sequential radiolabeling and hydrolysis reactions in a semiautomated system, equipped with a microwave, designed in our facilities for the synthesis of [^{18}F]flumazenil [12]. Five hot runs with 286.8–1953.6 MBq were performed. Following basic hydrolysis and purification by HPLC, the radiochemical yield of [^{18}F]FAG obtained at the end of synthesis was 9.7% ±2.8% end of bombardment (EOB) with a radiochemical purity of 98.7%±1.5% (Fig. 3). The total reaction time was reduced to only 62 min. The specific activity for [^{18}F]FAG was 18.09±2.9 GBq/μmol end of synthesis (EOS), and for [^{18}F]FDG, it was 1195±298 GBq/μmol (EOS).

3.2. In vitro E. coli uptake study

Fig. 4 shows the result of [^{18}F]FAG uptake by *E. coli*. In control group, the uptake of [^{18}F]FAG was increased with time. On the other hand, the uptake of [^{18}F]FAG was not changed in inhibition group. There was significant difference in uptake of [^{18}F]FAG between control and inhibition groups at 120 min (P<.05).

3.3. Biodistribution study

To compare the bioequivalence of [^{18}F]FAG synthesized by previous report [16], biodistribution study was performed in mice. Results show a biodistribution pattern of [^{18}F]FAG similar to previous report [16]. Fig. 5 shows the tissue distribution over time postinjection of [^{18}F]FAG. Radioactivity decreased rapidly with time in all tissues. For the first 60 min, radioactivity was concentrated in these organs involved in excretion and metabolism.

3.4. Small animal PET

PET imaging studies were performed in rats to allow a better visualization of abscess sites. In Fig. 6A, a red to yellow signal represents the accumulation of [^{18}F]FAG obtained in the right front leg muscle where *E. coli* was inoculated. Similar results were seen using [^{18}F]FDG. (Fig. 6B). When noninfectious inflammatory lesions were examined by the two radiocompounds, only [^{18}F]FDG clearly visualized the lesions (Fig. 6C, D).

The SUV values of these tracers in both sites are summarized in Table 3. The uptake of [^{18}F]FAG into target muscle (0.54±0.21, n=5) was significantly higher than that of [^{18}F]FAG into nontarget muscle (0.19±0.07 n=5) in infection model rats (P<.01). However, there was no significant difference between the uptake of [^{18}F]FAG into target (0.32±0.03, n=5) and nontarget areas (0.23±0.03,

Table 2
Hydrolysis yields of [^{18}F]FAG versus time at room temperature

NaOH concentration (M)	0.5 min	1 min	1.5 min	2 min	5 min	10 min
0.25	26.0±3.4	27.3±2.8	25.4±3.3	27.6±5.1	28.6±2.3	27.3±7.2
0.50	35.9±3.6	33.8±4.6	34.3±4.4	34.0±4.3	31.3±4.0	32.7±6.3
0.75	38.3±1.9	38.1±1.9	38.1±1.9	36.5±0.9	33.5±1.2	34.5±1.4
1.00	41.2±3.1	39.9±4.7	38.5±4.7	38.1±5.0	35.4±5.6	33.2±6.4
1.50	34.5±6.1	31.8±4.6	33.0±7.0	30.6±5.3	28.4±3.4	26.2±3.2

Values represent the mean±S.D. (n=3).

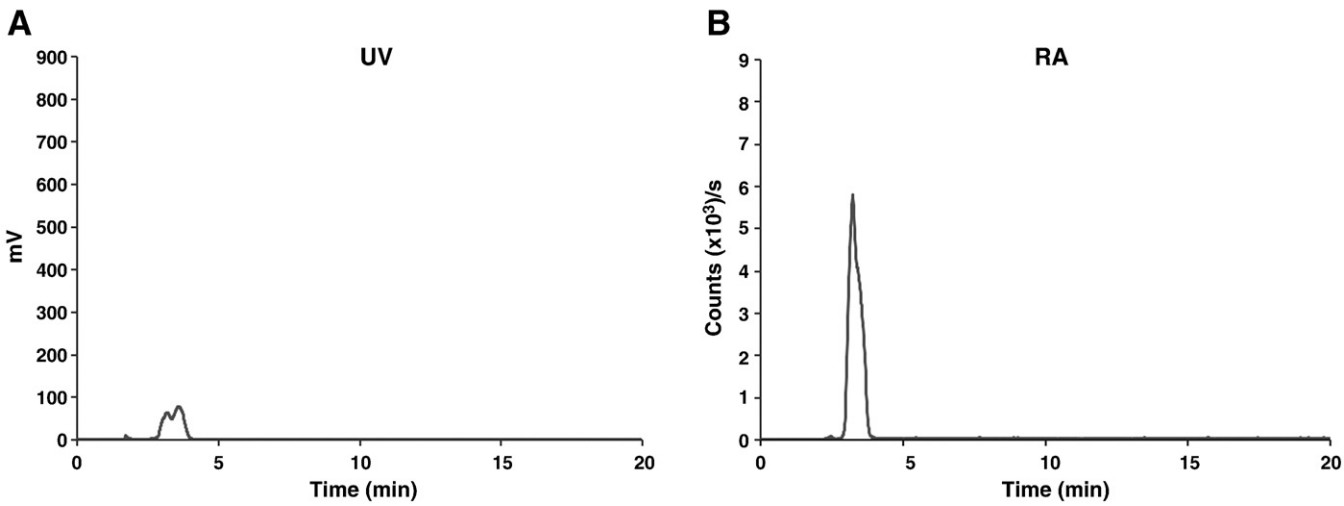

Fig. 3. HPLC chromatograms of [^{18}F]FAG on Cosmosil sugar-D column 4.6 mm ID×150 mm (A) UV at 210 nm; radioactivity (B).

n=5) in inflammation model rats. Furthermore, the uptake of [^{18}F]FAG into infection areas (0.54±0.21, *n*=5) was significantly higher than that of [^{18}F]FAG into inflammation areas (0.32±0.03, *n*=5, *P*<.05). In contrast, the uptake of [^{18}F]FDG into target muscle (infection: 1.58±0.12, *n*=5, inflammation: 1.36±0.30, *n*=5) was higher than that of [^{18}F]FDG into nontarget muscle (infection: 0.22±0.06, *n*=5, inflammation: 0.28±0.06, *n*=5) in both infection and inflammation model rats. Similarly, the uptake of [^{18}F]FDG in infection areas (1.58±0.12, *n*=5) was significantly higher than that of [^{18}F]FDG in inflammation areas (1.36±0.30, *n*=5, *P*<.05).

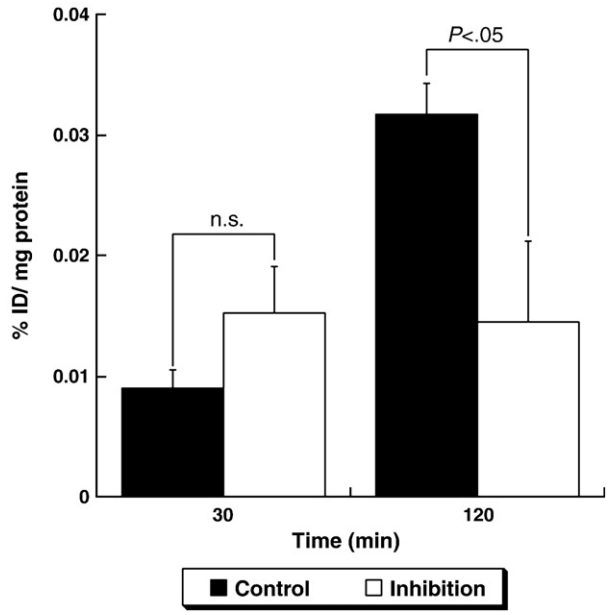

Fig. 4. Uptake of [^{18}F]FAG by *E. coli* in control and inhibition groups. The uptake was expressed as the percentage of the injected dose per miligram of protein (% ID/mg protein; mean±S.D, *n*=3).

3.5. Histology

As shown in Fig. 7A, small basophilic particles were scattered in the tissue injected with *E. coli*. The particles were confirmed as *E. coli* by immunostaining using anti–*E. coli* antibody (Fig. 8). Turpentine oil injection, a representative noninfectious inflammatory lesion, induced muscular necrosis with severe neutrophil infiltrations around the droplets (Fig. 7B).

4. Discussion

It has been an important issue in nuclear medicine to discriminate bacterial infection from nonbacterial inflammation, and several studies have been conducted to detect differences between molecular events in infection and inflammation in recent decades. Radiolabeled autologous leucocytes using [^{111}In]indium–oxine or [^{99m}Tc]technetium–hexamethylpropylene amine oxime (HMPAO) are the most common method for evaluating infection and inflammation in nuclear medicine [17,18]. However, it is difficult to distinguish bacterial infection from nonbacterial inflammation using these radiopharmaceuticals [1]. The antimicrobial peptide ^{99m}Tc-labeled ubiquicidin 29–41 is a promising radiopharmaceutical for distinguishing bacterial infection from nonbacterial inflammation [19]. The use of radiolabeled antimicrobial peptides to images infection and the suggestion that they can differentiate infection from inflammation have been reviewed by Nibbering et al. [20]. Among PET radiopharmaceuticals, [^{18}F]FDG was applied for bacterial infection because the processes of bacterial infection show increased glycolysis. However, even when [^{18}F]FDG is exquisitely sensitive, its specificity is low, and it accumulates in a variety of conditions including malignant and benign neoplasm, fractures and nonbacterial inflammation as well as bacterial infection. Although F-18–labeled ciprofloxacin has been reported as a infection-specific

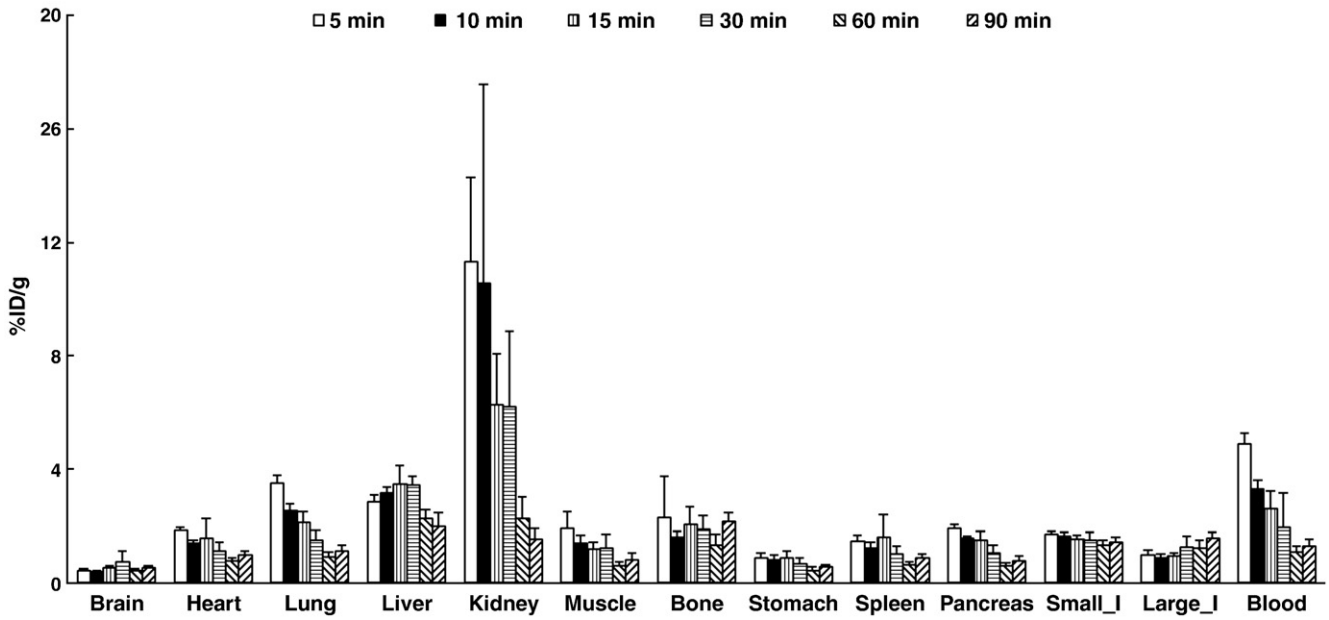

Fig. 5. Tissue biodistribution of [^{18}F]FAG in mice (n=5 for each time) by the dissection method. Radioactivity was expressed as the percentage of the injected dose per gram of tissue or organ (% ID/g; mean±S.D, n=5).

radiopharmaceutical, contradicting results have also been reported that [^{18}F]ciprofloxacin had no specific binding to bacteria [21] and poor retention in bacteria-infected tissues in patients [22]. Thus, the search for better radiopharmaceuticals to distinguish between infection and inflammation is ongoing. In this study, we hypothesized that F-18–labeled *N*-acetylglucosamine derivatives were suitable radiopharmaceuticals for distinguishing bacterial infection from nonbacterial inflammation, and [^{18}F]FAG was designed as a candidate radiopharmaceutical.

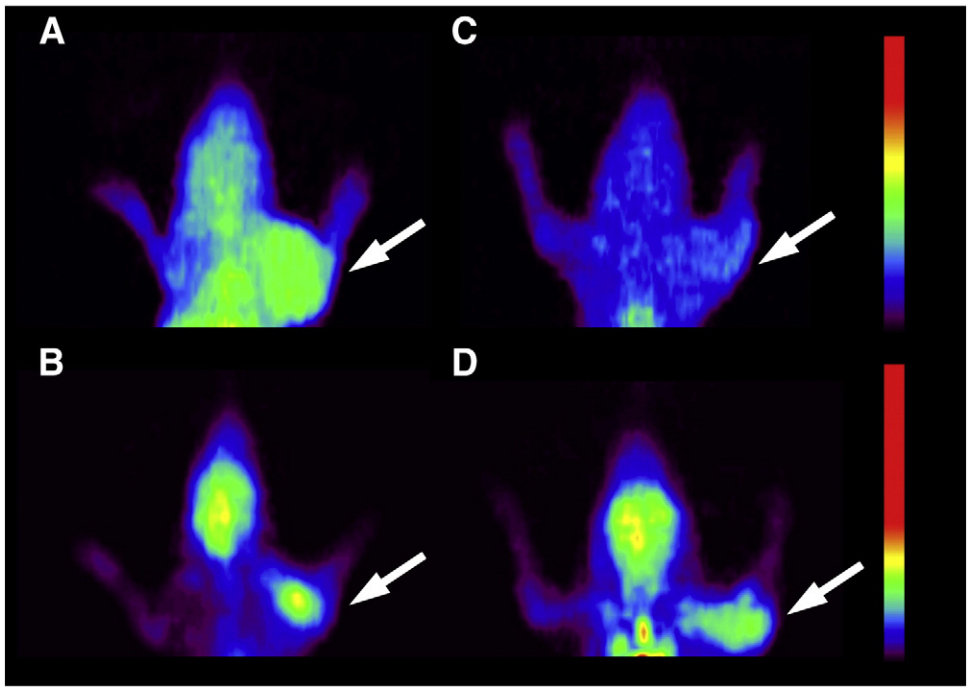

Fig. 6. Representative static maximun intensity projection (MIP) PET images on rats with an induced bacterial infection or nonbacterial inflammation in the right front leg muscle. Images were acquired 60 min after intravenous injection of 16.7–22.2 MBq of [^{18}F]FAG or [^{18}F]FDG. Arrow indicates infection or inflammation sites (animals positioned prone on imaging table). (A) Infection model after injection of [^{18}F]FAG. (B) Infection model after injection of [^{18}F]FDG. (C) Inflammation model after injection of [^{18}F]FAG. (D) Inflammation model after injection of [^{18}F]FDG. The same scale is used in the images of the same row.

Table 3
SUV values of [^{18}F]FAG and [^{18}F]FDG in bacterial infection and nonbacterial inflammation areas

Model	Bacterial infection (SUV)		Nonbacterial inflammation (SUV)	
	Target areas	Nontarget areas	Target areas	Nontarget areas
[^{18}F]FAG	0.54±0.21*,#	0.19±0.07	0.32±0.03	0.23±0.03
[^{18}F]FDG	1.58±0.12**,#	0.22±0.06	1.36±0.30**	0.28±0.06

Values represent the mean±S.D. (n=5).
* P<.01 vs. the nontarget areas in infection model.
** P<.001 vs. the nontarget areas in infection or inflammation model.
# P<.05 vs. the target areas in inflammation model.

To realize [^{18}F]FAG-PET in a clinical situation, we developed a simple radiosynthesis method of [^{18}F]FAG by using a new precursor and microwave heating in this study. The radiosynthesis of [^{18}F]FAG has been previously reported for tumor imaging [23,24]. However, in the previous method, the three-step reaction led to longer total reaction times, and the complex purification procedure to eliminate pyridine made it difficult to apply for clinical purposes. We designed a two-step semiautomated radiosynthesis system consisting of incorporation of [^{18}F]F$^-$ using microwave irradiation and basic hydrolysis. After purification, radiochemical purity of [^{18}F]FAG was more than 98%, the radiochemical yield was about 9.7% (EOB) and the total reaction time was 62 min. The obtained final radiochemical yield of [^{18}F]FAG was lower considering the incorporation yields (75.5%±4.2%) and hydrolysis (30%-40%) yields. Considerable radioactivity was remained inside the preparative column during purification of the crude product. This may be the main reason for this discrepancy. Although further investigation regarding purification would be needed, these results allow us to obtain [^{18}F]FAG.

Addition of glucosamine has been reported to inhibit acetylglucosamine pathway [25]. After a 120-min incubation, the uptake of [^{18}F]FAG by *E. coli* cells was reduced significantly. This results support the hypothesis that [^{18}F]FAG can be incorporated into the bacterial cell walls.

In the biodistribution of [^{18}F]FAG in mice, immediately after injection of [^{18}F]FAG, transient accumulations of radioactivity in the kidney, liver and blood were observed, but after 60 min, almost all of these radioactivities became low. The highest uptake in the kidney at 5 min reflected the rapid urinary excretion of [^{18}F]FAG. The other organs showed no significant uptake, and the rapid clearance offered

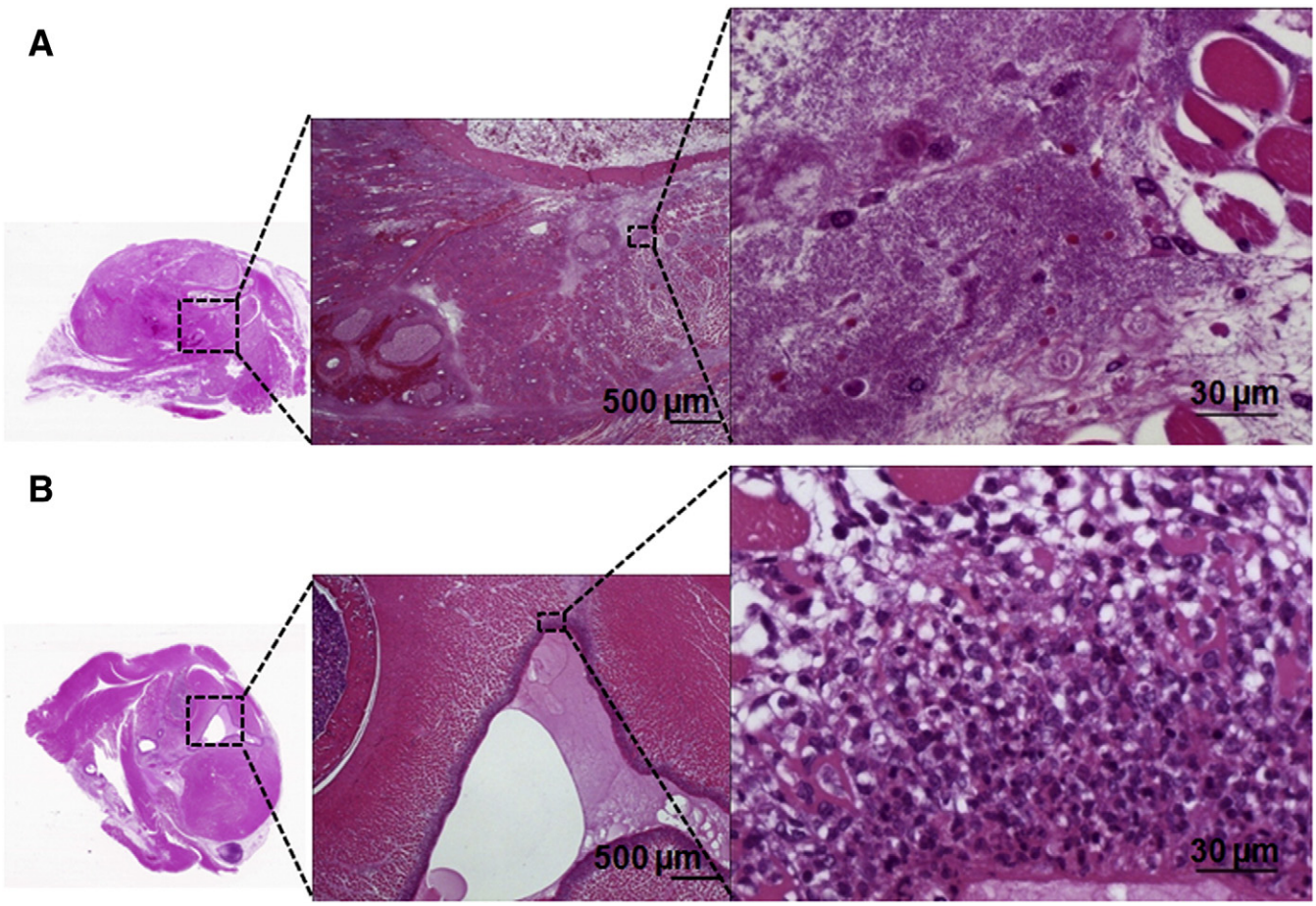

Fig. 7. Hemotoxylin and eosin tissues staining from correspondingly resected muscular samples at radiotracer acummulation site. (A) Rat injected with *E. coli* in the right front leg muscle. (B) Rat injected with turpentine oil in the right front leg muscle.

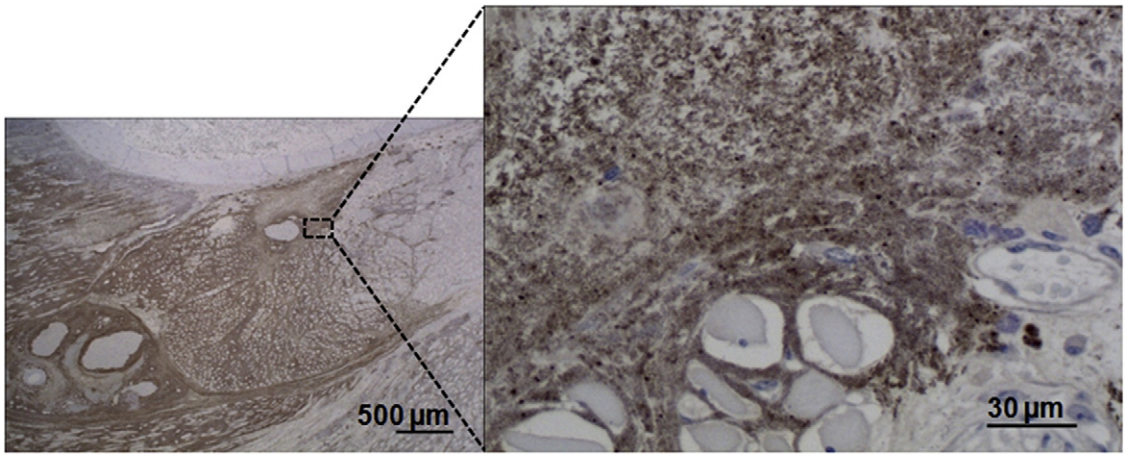

Fig. 8. Detection of *E. coli* in the correspondingly resected muscular sample of a rat injected with the bacterial cells in the right front leg muscle. Anti–*E. coli* immunostaining confirmed the existence of the microbes as brown-stained dots on the slide section.

lower background levels during image acquisition. The biodistribution results indicated the bioequivalence of newly synthesized [^{18}F]FAG with *N*-acetyl-D-[1-^{14}C]glucosamine and [^{18}F]FAG as previously reported [16]. Based on the biodistribution data, the accumulation pattern of [^{18}F]FAG would be suitable for distinguishing bacterial infection from inflammation due to its low background accumulation.

Finally, using small animal PET, we demonstrated that [^{18}F]FAG accumulation was significantly higher in bacterial infection compared with nonbacterial inflammation. Actually, [^{18}F]FAG clearly visualized the *E. coli*–induced infection areas but not nonbacterial inflammation areas. These results indicated that [^{18}F]FAG had the ability to discriminate the infection areas from the inflammation areas. The uptakes of [^{18}F]FDG into both infection and inflammation areas were significantly higher than those of [^{18}F]FDG into nontarget areas. These results of [^{18}F]FDG were consistent with previous reports [26] and suggested that it was difficult to distinguish the infection areas from inflammation areas with [^{18}F]FDG.

In the histological analysis, the presence of *E. coli* was confirmed in the infection areas but not in the inflammation areas. This was consistent with the result of PET study of [^{18}F]FAG and suggested that [^{18}F]FAG could be incorporated into bacterial cells. Further histological analysis of the infection areas showed gross infiltration of granulocytes and macrophages, while turpentine oil-induced inflammation areas showed abscess formation with neutrophils and macrophages surrounding the abscess wall. This may be the reason why [^{18}F]FDG cannot easily distinguish infection from inflammation areas [27].

5. Conclusion

Using TA-BrAG as a precursor, a new radiosynthesis method of [^{18}F]FAG was achieved with fewer steps and a shortened synthesis time than previously reported. Furthermore, [^{18}F]FAG was able to distinguish infection from inflammation. To best of our knowledge, present study is the first trial to evaluate the *N*-glucosamine derivative as a bacterial infection PET imaging agent. The mechanisms of uptake for [^{18}F]FAG in infected tissue still require to be studied in-depth, but these promising findings will encourage future works with *N*-glucosamine derivatives.

Acknowledgments

This study was supported by the 21st Century COE program and research grants (09-92-181 and 20591199) from the Ministry of Education, Culture, Sports, Science and Technology of Japan. We thank Mr. Toshinao Nakakoji and Mr. Akira Ito of CMI for carrying out the [^{18}F]fluoride production and Dr. Talakad Lohith for preliminary PET study support.

References

[1] Palestro CJ. Radionuclide imaging of infection: in search of the grail. J Nucl Med 2009;50:671–3.
[2] Rakesh K, Murali RN, Balakrishnan V, Chandershekar B, Arun M. FDG-PET imaging in infection and inflammation. IJNM 2006;21:104–13.
[3] Rakesh K, Sandip B, Drew T, Vivek A, Hongming Z, Abass A. Role of modern imaging techniques for diagnosis of infection in the era of ^{18}F-fluorodeoxyglucose positron emission tomography. Clin Microbiol Rev 2008;21:209–24.
[4] Oyen WJ, Corstens FHM, Boerman OC. Discriminating infection from sterile inflammation: can radiolabelled antibiotics solve the problem? Eur J Nucl Med Mol Imaging 2005;32:151–2.
[5] Mengin-Lecreulx D, van Heijenoort J. Identification of the glmU gene encoding *N*-acetylglucosamine-1-phosphate uridyltransferase in *Escherichia coli*. J Bacteriol 1993;175:6150–7.
[6] Plumbridge J, Vimr E. Convergent pathways for utilization of the amino sugars *N*-acetylglucosamine, *N*-acetylmannosamine, and *N*-acetylneuraminic acid by *Escherichia coli*. J Bacteriol 1999;181:47–54.
[7] Maley F, Lardy H. Synthesis of *N*-substituted glucosamines and their effect on hexokinase. J Biol Chem 1955;214:765–73.

[8] Dwek R, Kent P, Xavier A. *N*-Fluoroacetyl-D-glucosamine as a molecular probe of lysozyme structure by using [^{19}F]fluorine-nuclear-magnetic resonance techniques. E J Biochem 1971;23:343–8.

[9] Berki A, Szarek M, Plenkiewicz J, Szarek W, Kisilevsky R. Synthesis of 4-deoxy analogues of 2-acetamido-2-deoxy-D-glucose and 2-acetamido-2-deoxy-D-xylose and their effects on glycoconjugate biosynthesis. Carbohydr Res 2000;325:30–45.

[10] Signore A, Mather S, Piaggio G, Malviya G, Dierckx R. Molecular imaging of inflammation/infection: nuclear medicine and optical imaging agents and methods. Chem Rev 2010;110:3112–45.

[11] Myszka H, Bednarczyk D, Najder M, Kaca W. Synthesis and induction of apoptosis in B cell chronic leukemia by diosgenyl 2-amino-2-deoxy-β-D-glucopyranoside hydrochloride and its derivatives. Carbohydr Res 2003;338:133–41.

[12] Mandap K, Ido T, Kiyono Y, Kobayashi M, Lohith T, Mori T, et al. Development of microwave-based automated nucleophilic [^{18}F] fluorination system and its application to the production of [^{18}F] flumazenil. Nucl Med Biol 2009;36:403–9.

[13] Gomzina N, Vasil'ev D, Krasikova R. Optimization of 2-[^{18}F]fluoro-2-deoxy-D-glucose involving base hydrolysis. Radiochem 2002;44:403–9.

[14] Yamada R, Watanabe M, Omura T, Sato N, Shimizu K, Takahashi M. Development of a small animal PET scanner using DOI detectors. IEEE Trans Nucl Sci 2008;55:906–11.

[15] Inai K, Takagi K, Takimoto N, Okada H, Imamura Y, Ueda T, et al. Multiple inflammatory cytokine-productive ThyL-6 cell line established from a patient with thymic carcinoma. Cancer Sci 2008;99:1778–84.

[16] Fujiwara T, Kubota K, Sato T, Matsuzawa T, Tada M, Iwata R, et al. *N*-[^{18}F]fluoroacetyl- D-glucosamine: a potential agent for cancer diagnosis. J Nucl Med 1990;31:1654–8.

[17] Kjaer A, Lebech AM. Diagnostic value of ^{111}In-granulocyte scintigraphy in patients with fever of unknown origin. J Nucl Med 2002;43:140–4.

[18] Filippi L, Uccioli L, Giurato L, Schillaci O. Diabetic foot infection: usefulness of SPECT/CT for ^{99m}Tc–HMPAO-labeled leukocyte imaging. J Nucl Med 2009;50:1042–6.

[19] Welling M, Paulusma-Annema A, Balter H, Pauwels E, Nibbering P. Technetium-99m labelled antimicrobial peptides discriminate between bacterial infections and sterile inflammations. Eur J Nucl Med 2000;27:292–301.

[20] Nibbering P, Welling M, Van den Broek P, Van Wyngaarden K, Pauwels E, Calame W. Radiolabelled antimicrobial peptides for imaging of infections: a review. Nucl Med Commun 1998;19: 1117–21.

[21] Zijlstraa S, Gunawana J, Freytagb C, Burchert W. Synthesis and evaluation of fluorine-18 labelled compounds for imaging of bacterial infections with pet. Appl Radiat Isot 2006;64:802–7.

[22] Langer O, Brunner M, Zeitlinger M, Ziegler S, Müller U, Dobrozemsky G, et al. In vitro and in vivo evaluation of [^{18}F] ciprofloxacin for the imaging of bacterial infections with PET. Eur J Nucl Med Mol Imaging 2005;32:143–50.

[23] Tada M, Atsushi O, Iwata R, Fujiwara T, Kubota K, Matsuzawa T, et al. An efficient, one-pot synthesis of 2-deoxy-2-[^{18}F]fluoroacetamido-D-glucopyranose (*N*-[^{18}F]fluoroacetyl- D-glucosamine), potential diagnostic imaging agent. J Label Compd Radiopharm 1989;27:1317–24.

[24] Tada M, Atsushi O, Iwata R, Sato K, Kubota K, Fujiwara T, et al. A rapid and efficient synthesis of 2-deoxy-2-[^{18}F]fluoroacetamido-D-mannopyranose and -D-galactopyranose. J Label Compd Radiopharm 1990;28:848–54.

[25] Asensio C, Ruiz-Amil M. *N*-Acetyl-D-glucosamine kinase. II. *Escherichia coli*. Methods Enzymol 1966;9:421–5.

[26] Yamada S, Kubota K, Kubota R, Ido T, Tamahashi N. High accumulation of fluorine-18-fluorodeoxyglucose in turpentine-induced inflammatory tissue. J Nucl Med 1995;36:1301–6.

[27] Kubota R, Yamada S, Kubota K, Ishiwata K, Tamahashi N, Ido T. Intratumoral distribution of fluorine-18-fluorodeoxyglucose in vivo: high accumulationin macrophages and granulationtissues studied by microautoradiography. J Nucl Med 1992;33: 1972–98.